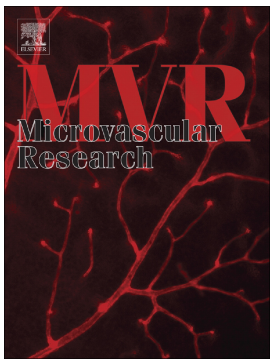

Image-based spatio-temporal model of drug delivery in a heterogeneous vasculature of a solid tumor — Computational approach

Farshad M. Kashkooli, M. Soltani, M. Rezaeian, Erfan Taatizadeh, Mohammad-Hossein Hamedi

PII: S0026-2862(18)30096-7
DOI: https://doi.org/10.1016/j.mvr.2019.01.005
Reference: YMVRE 3858

To appear in: *Microvascular Research*

Received date: 6 September 2018
Revised date: 29 January 2019
Accepted date: 29 January 2019

Please cite this article as: F.M. Kashkooli, M. Soltani, M. Rezaeian, et al., Image-based spatio-temporal model of drug delivery in a heterogeneous vasculature of a solid tumor — Computational approach, Microvascular Research, https://doi.org/10.1016/j.mvr.2019.01.005

Image-based spatio-temporal model of drug delivery in a heterogeneous vasculature of a solid tumor— Computational approach

Farshad M. Kashkooli[1], M. Soltani[1,2,3,4,5,*], M. Rezaeian[1], Erfan Taatizadeh[1], Mohammad-Hossein Hamedi[1]

[1] Department of Mechanical Engineering, K. N. Toosi University of Technology, Tehran, Iran

[2] Advanced Bioengineering Initiative Center, Computational Medicine Center, K. N. Toosi University of Technology, Tehran, Iran

[3] Department of Electrical and Computer Engineering, University of Waterloo, ON, Canada

[4] Centre for Biotechnology and Bioengineering (CBB), University of Waterloo, Waterloo, Ontario, Canada

[5] Cancer Biology Research Center, Cancer Institute of Iran, Tehran University of Medical Sciences, Tehran, Iran

* Corresponding author:

M. Soltani, University of Waterloo, 200 University Ave. Waterloo, Ontario, Canada, N2L3G1,

Tel./Fax: +1 (519) 888-4567, Email address: msoltani@uwaterloo.ca

Abstract

The solute transport distribution in a tumor is an important criterion in the evaluation of the cancer treatment efficacy. The fraction of killed cells after each treatment can quantify the therapeutic effect and plays as a helpful tool to evaluate the chemotherapy treatment schedules. In the present study, an image-based spatio-temporal computational model of a solid tumor is

provided for calculation of interstitial fluid flow and solute transport. Current model incorporates heterogeneous microvasculature for angiogenesis instead of synthetic mathematical modeling. In this modeling process, a comprehensive model according to Convection-Diffusion-Reaction (CDR) equations is employed due to its high accuracy for simulating the binding and the uptake of the drug by tumor cells. Based on the velocity and the pressure distribution, transient distribution of the different drug concentrations (free, bound, and internalized) is calculated. Then, the fraction of killed cells is obtained according to the internalized concentration. Results indicate the dependence of the drug distribution on both time and space, as well as the microvasculature density. Free and bound drug concentration have the same trend over time, whereas, internalized and total drug concentration increases over time and reaches a constant value. The highest amount of concentration occurred in the tumor region due to the higher permeability of the blood vessels. Moreover, the fraction of killed cells is approximately 78.87% and 24.94% after treatment with doxorubicin for cancerous and normal tissues, respectively. In general, the presented methodology may be applied in the field of personalized medicine to optimize patient-specific treatments. Also, such image-based modeling of solid tumors can be used in laboratories that working on drug delivery and evaluating new drugs before using them for any *in vivo* or clinical studies.

Keywords: Drug delivery, Solid tumor, Microvasculature, Image-based spatio-temporal model, Heterogeneous capillary network, Fraction of killed cells, Mathematical modeling.

Introduction

Cancer is one of the major public health problems all over the world (Zhang et al., 2014, 2015). The key to successful cure of tumor is mostly an efficient delivery of anticancer drugs after the surgery (Soltani and Chen, 2011). In solid tumors, physiological barriers such as high

density of extracellular matrix (ECM), solid stress elevation/vessel compression, and leaky and irregularly shaped microvascular networks are the main reasons in decreasing the efficacy of drug delivery and treatment (Stylianopoulos et al., 2018; Dewhirst and Secomb, 2017). These barriers and also the lack of lymphatic system have contribution in high values of interstitial fluid pressure (IFP). Elevated IFP prevents the systematic drug delivery by an outward convection against inward drug diffusion (Stylianopoulos et al., 2018; Dewhirst and Secomb, 2017; Jain and Baxter; 1988, Soltani and Chen, 2011). Each tumor has its own structure and physiochemical characteristics such as surface per volume of vasculatures, capillary networks pattern, and hydraulic conductivity to name a few. This makes drug delivery and therefore, treatment of solid tumor very complicated and case specific. On the other hand, quantitative prediction of drug delivery to solid tumor using patient-specific data is noteworthy in clinical decision for therapeutic planning (Meghdadi et al., 2016). The aim of mathematical modeling and simulation is to better understand the tumor behaviors which will ultimately improve the treatment outcome.

Due to the multiple processes involved in drug delivery and tumor microenvironment complexity, mathematical modeling is an effective tool to find out the restriction agents of inefficient anti-cancer drug delivery. There exist two major methodologies to simulate delivery of drugs to solid tumors: macroscopic and microscopic. In the first approach, distribution of variables including interstitial fluid velocity (IFV), IFP, and drug concentration over the tumor radius length-scale is significant. In the second one, some characteristics such as microvascular network structure, blood flow within microvessels, and interaction between blood flow and microvascular wall are incorporated in the model. Following macroscopic approach, Baxter and Jain (1989, 1990, 1991) applied a continuous porous medium model to investigate the influences

of different factors on the drugs concentration in ECM of solid tumors. Soltani and Chen (2011, 2013) improved the mathematical model and applied it to investigate two new parameters of spherical tumors: critical radius of the tumor and critical radius of the necrotic zone. Also, to study the shape and size effects of tumors on drug delivery, they applied the model to different geometries (Soltani, 2012; Soltani and Chen, 2012; Soltani et al., 2014). El-Kareh and Secomb (2005) and Eikenberry (2009) used a mathematical model tool to determine the drug concentration respectively in the extracellular and intracellular spaces of solid tumors. There exist many new efforts in mathematical modeling and simulation of drug delivery to solid tumors, in the literature (Pishko et al., 2011; Sefidgar et al., 2014a, 2014b, 2015, Asgari et al., 2018; Soltani et al., 2017; Chou et al., 2017; Zhan and Xu, 2013; Zhan et al., 2014, 2017; Stylianopoulos et al., 2015; Mpekris et al., 2017; Steuperaert et al., 2017; Shamsi et al., 2018) to study the effect of different factors and parameters including IFP, IFV, capillary network, and concentration.

Tumor microvasculature is blood vessels which provide nutrients, oxygen or glucose for growth of the tumor (Baxter and Jain, 1989). Various studies have been developed on the vascular structure and formation of the capillaries around the tumor. Most of these studies used a mathematical modeling to generate tumor microvasculature based on the work of Anderson et al. (1998, 2012). Anderson and Chaplain (1998) developed an angiogenesis model, in which new vessels began to grow from a parent vessel in keeping with a special probability calculated according to physiological conditions such as concentration of VEGF and density of endothelial cells. Welter et al. (2008, 2009, 2010) by considering some phenomena including co-option of adjacent vasculature to the tumor, growth of the tumor, and collapse of the vessels, developed remodeling of microvascular structure. Zhang (2018) modeled the fluid flow in two types of

capillary channels: a narrow constricted capillary and a leaky one. Recently, Stephanou et al. (2005), J. Wu et al. (2008), Welter and Rieger (2013), M. Wu et al. (2014), Sefidgar et al. (2015), and Soltani et al. (2017) simulated the drug delivery to solid tumors in the presence of heterogeneous microvasculature but their mathematical approach is not absolutely accurate and real. These models are helpful for investigating the interaction of various physiological phenomena within the tumor during drug transport; however, they cannot accurately predict the tumor behavior in a specific patient, as the tumor microenvironment changes widely from one case to another. Therefore, unlike these synthetic microvascular mathematical models, an imaged-based approach is employed to calculate the spatio-temporal distribution of the drug within the tumor in the present study.

Medical images are the most common resources of clinical data which are used in personalized models. Recent computational fluid dynamics (CFD) methodologies for modeling the drug delivery to solid tumors have generated a novel domain of personalized clinical possibilities by integrating more patient-specificity with the medical imaging data. Some of these previously published investigations used magnetic resonance imaging (MRI) such as the works of Bhandari et al. (2018) and Tan et al. (2003) for brain tumor or Pishko et al. (2011) for mice tumor. No one of the literature studies used the image-based geometry of the capillary networks as their main geometry and instead, only the mathematical modeling has been used to generate a synthetic capillary network. Using image-based geometry for capillaries in CFD simulations, can help researchers to better understand *in vivo* model behavior. Nevertheless, capturing an image of the capillaries is one of the main challenges because of two major problems: first, the way of capturing an image of the capillaries with existent medical devices where their accuracy cannot provide microvasculature precisely and second, the way of using capillaries as a geometry in

CFD analysis. There exist several investigations and algorithms proposed to detect the microvasculature from an image which contain the capillary network and also, a noisy background, for example, single-scale and multi-scale matched filters (Chaudhuri et al., 1989; Zhang et al., 2010; Malek et al., 2015; Sofka and Stewar; 2005), single-scale and multi-scale Gabor filters (Rangayyan et al., 2007; Janko et al., 2005), and bar-selective combination of shifted filter responses (Strisciuglio et al., 2015). Abdallah et al. (2015) proposed a novel algorithm for detection of the retinal vascular tree which eliminate some noises in the image and connect discontinuity among the blood vessels.

An image-based spatio-temporal solid tumor model can be applied to optimize and evaluate the treatment strategies for patient-specific therapies. In the current study, for the first time, a comprehensive approach for solving transport phenomenon of the chemotherapy, based on CDR equations, was combined with an image-based method to evaluate the drug delivery to solid tumor by considering the heterogeneous microvasculature network. The methodology is such that using an image-processing method, the tumor geometry was reconstructed from a previously obtained image, and then, the numerical simulations were performed. First, IFP and IFV were calculated in both microvascular network and interstitium, simultaneously. Then, different drug concentrations including free, bound, and internalized were obtained. Eventually, using the predicted intracellular drug concentration, the fraction of killed cells parameter was obtained and subsequently, anticancer drug efficacy and side effects of the drug on normal tissue were evaluated. This research provides a preliminary step forward towards the goal of personalized medicine.

2. Materials and Methods

In the current study, an image-based model employed to study the drug delivery process

in solid tumors. Mathematical modeling approach, image-processing procedure, model geometry, computational domain, boundary conditions, model parameters, solution strategy, and eventually grid independency test are investigated in the following sections.

2.1. Mathematical modeling procedure

The chemotherapy drugs (in this study, doxorubicin) are transmitted to the site of the tumor via the blood vessels. Then, they pass through the wall of the tumor vessel and after that, they travel the remaining distance from the vessel wall to the cancer cells. Free molecules of doxorubicin in tumor interstitial space can bind to receptors of the cell surface, unbind or get internalized (Soltani et al., 2017; Stylianopoulos et al., 2015). Fig. 1 represents the mentioned mechanisms of drug delivery considered in present study.

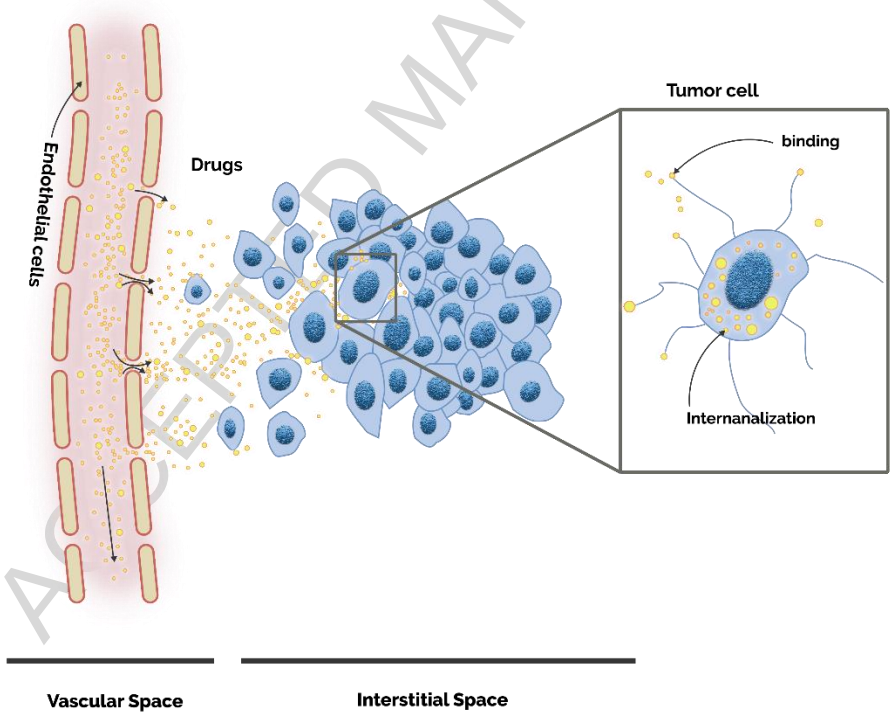

Fig. 1. Schematic of the drug delivery mechanism considered in the present study

The overall model for solute transport, which is called CDR model, consists of: drug transport across the vessels due to the diffusion and convection, drug transport in interstitial

space by diffusion and convection in tissue, and other mechanisms including drug binding to cancer cells and its internalization into the cells. Details of these equations are mentioned in the literature (Baxter and Jain, 1991; Sefidgar et al., 2015; Soltani et al., 2014, 2017; Stylianopoulos and Jain, 2013). This modeling is based on compartment models which are widely used to describe the drug delivery, as they are enable to quantify the biochemical and physiological phenomena (Soltani et al., 2017). In compartmental modeling, it is assumed that the concentration in each compartment is distributed independently. But, CDR equations supposed that the drug concentration in the second compartment is changing because of diffusion and convection processes and this is the difference between these two models (Soltani et al., 2017). In other words, the spatio-temporal distribution is added to the compartmental modeling in the present study. So, the drug distribution in compartments relies on both space and time. The block-diagram of the current study model is shown in Fig. 2.

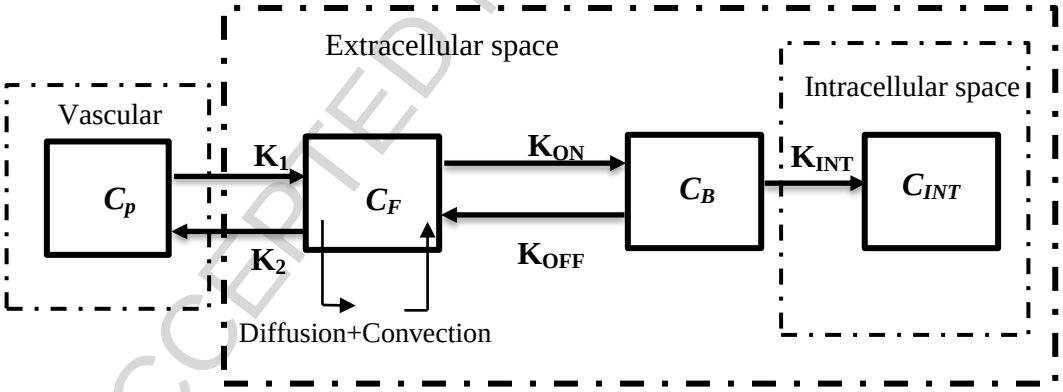

Fig. 2. Drug transport modeling of current study based on 5-K compartment model

The equation system applied for the drug transport in interstitial space is as following (Soltani et al., 2017; Stylianopoulos et al., 2015):

$$\frac{\partial C_F}{\partial t} = -v\nabla C_F - D\nabla^2 C_F - \frac{1}{\varphi} K_{ON} C_{rec} C_F + K_{OFF} C_B + (\Phi_V - \Phi_L) \qquad \text{Free drug} \qquad (1)$$

$$\frac{\partial C_B}{\partial t} = \frac{1}{\varphi} K_{ON} C_{rec} C_F - K_{OFF} C_B - K_{INT} C_B \quad \text{Bound drug} \quad (2)$$

$$\frac{\partial C_{INT}}{\partial t} = K_{INT} C_B \quad \text{Internalized drug} \quad (3)$$

where, C_F, C_B, and C_{INT} are the free, bound, and internalized drug concentration, respectively. C_{rec} is the concentration of cell surface receptors, v is the IFV obtained from Darcy's law, D is the coefficient of diffusion, K_{ON}, $K_{OFF,}$ and K_{INT} are respectively the constants of association, dissociation, and internalization rate and also, φ is the volume fraction of tumor accessible to the drug. Φ_V and Φ_L are respectively the solute transport rates per unit volume from blood vessels into the interstitium (like a leakage from a capillary (Zhang, 2018)), and from the interstitium into the lymphatic vessels. These two parameters are obtained as following by Kedem-Katchalsky equation (Curry, 1984; Jain, 1997):

$$\Phi_V = \phi_V (1-\sigma_f) C_p + \frac{PS}{V}(C_p - C)\frac{Pe}{e^{Pe}-1} \quad (4)$$

$$\Phi_L = \begin{cases} \phi_L C & \text{Normal Tissue} \\ 0 & \text{Tumor Tissue} \end{cases} \quad (5)$$

where,

$$Pe = \frac{\phi_V (1-\sigma_f) V}{PS} \quad (6)$$

ϕ_V is the source term expressed the extravasation from microvessels, and ϕ_L is the drainage term represented the elimination by the lymphatic system. These parameters are defined as bellows:

$$\phi_V = \frac{J_V}{V} = \frac{L_p S}{V}(P_B - P_i - \sigma_s(\pi_B - \pi_i)) \quad (7)$$

$$\phi_L = \frac{L_{pL} S_L}{V}(P_i - P_L) \quad (8)$$

In the modeling of fluid flow, three fronts are noteworthy: blood flow in microvessels, fluid flow in lymphatic systems, and fluid flow in interstitium. Fluid flow in tissue is considered in CDR equation. Here, the tissue is considered as a porous medium. For fluid transport in tissue, Darcy's law is used. In the current study, the IFV is calculated by Darcy's equation, as bellowing:

$$v_i = -\kappa \nabla P_i \tag{9}$$

while, the IFP is calculated as follows:

$$-\kappa \nabla^2 P_i = \phi_V - \phi_L \tag{10}$$

The procedure of calculating the IFP is exactly explained in the previous works of our group (Soltani and Chen, 2013; Soltani et al., 2017).

Using the predicted intracellular drug concentration (C_{INT}), efficacy of anticancer drug and also, side effects of chemotherapy on normal tissue are evaluated according to the previously measured experimentally formulation for doxorubicin (Kerr et al., 1986). Results were fitted to an exponential expression as the function of C_{INT}. In other words, S_F is the fraction of surviving cells which is calculated as following (Mpekris et al., 2017):

$$S_F = \exp(-\omega \cdot C_{INT}) \tag{11}$$

in which, ω is a fitting parameter defined in literature (Kerr et al., 1986) for doxorubicin and C_{INT} is the intracellular concentration of the doxorubicin.

Summaries of model parameters of interstitial transport and also, solute transport for tumor and normal tissue used in the numerical simulations are listed in Table 1 and Table 2.

Table 1 Interstitial transport parameters for tumor and normal tissue used in simulation

Parameter	Description	Value	References
π_b [mmHg]	Capillary oncotic pressure	20 (Normal) 20 (Tumor)	Soltani and Chen (2011) & Sefidgar et al. (2014a)
π_i [mmHg]	Interstitial fluid oncotic pressure	10 (Normal) 15 (Tumor)	Soltani and Chen (2011) & Sefidgar et al. (2014a)
$(S/V)_L$ [1/cm]	Lymphatic surface area per unit volume for transport	70 (Normal) 20 (Tumor)	Chou et al. (2017)
σ_s	Average osmotic reflection coefficient	0.91 (Normal) 0.82 (Tumor)	Soltani and Chen (2011) & Sefidgar et al. (2014a)
L_p [cm/((mmHg)*s)]	Hydraulic conductivity of the microvascular wall	0.36e-7 (Normal) 2.8e-7 (Tumor)	Soltani and Chen (2011) & Sefidgar et al. (2014a)
κ [cm^2/(mmHg*s)]	Interstitium hydraulic conductivity	8.53e-9 (Normal) 4.13e-8 (Tumor)	Soltani and Chen (2011) & Sefidgar et al. (2014a)

Table 2. Solute transport parameters used in simulation

Parameter	Description	Value	References
D_{eff} [cm^2/s]	Effective diffusion coefficient	1.58e-6 (Normal) 3.40e-6 (Tumor)	Chou et al. (2017) & Zhan et al. (2014)
P_m [cm/s]	Microvessel permeability coefficient	3.75e-5 (Normal) 3.00e-4 (Tumor)	Chou et al. (2017) & Zhan et al. (2014)
σ_f	Filteration reflection coefficient	0.9	Soltani and Chen (2011) & Sefidgar et al. (2014a)
K_{ON} [1/(M·s)]	Constant of binding rate	1.5e3	Stylianopoulos et al. (2015) & Stylianopoulos and Jain (2013)
K_{OFF} [1/s]	Constant of unbinding rate	8e-3	Stylianopoulos et al. (2015) & Stylianopoulos and Jain (2013)
K_{INT} [1/s]	Constant of cell uptake rate	5e-5	Stylianopoulos et al. (2015) & Stylianopoulos and Jain (2013)
φ	Tumor volume fraction accessible to drugs	0.4	Zhan and Xu (2013)
C_{rec} [M]	Concentration of cell surface receptors	1e-5	Stylianopoulos et al. (2015)
P_L [Pa]	Hydrostatic pressure of lymphatic vessels	0	Soltani and Chen (2011) & Sefidgar et al. (2014a)
ω [m^3/mole]	Cancer cell survival constant	0.6603	Mpekris et al. (2017)

2.2. Image-processing procedure of the input image

The first step for the creation of the 2-dimensional geometry from an image consisted the capillaries, is image-processing which is consisted some crucial steps to improve the contrast and quality of input image. Basically, raw input RGB images have noises, low contrast, and homogeneous colors. Consequently, some image-processing techniques such as histogram equalization of color intensity and removing details by making a binary image (black and white image), must be taken into account to capture the microvasculature area from a background of the image more effectively. In the final step, the contour of the processed image is evaluated and the minimum values of them are used to create the closed surface from them which in reality is the capillaries. Step by step descriptions of image-processing procedure applied to input image are explained in Fig. 3. Furthermore, it is worth mentioning that due to the lack of availability of clinical image and data set with a high resolution, the synthetic image from the research of Welter et al. (2009) is employed in current study. In the study of Welter et al. (2009), each lattice site of the space occupied by a tumor is identified with one tumor cell. A lattice site which was occupied by a tumor cell in the past represents cancerous tissue, otherwise unoccupied sites represent normal tissue. In this way, the tumor region can be distinguished from normal sites.

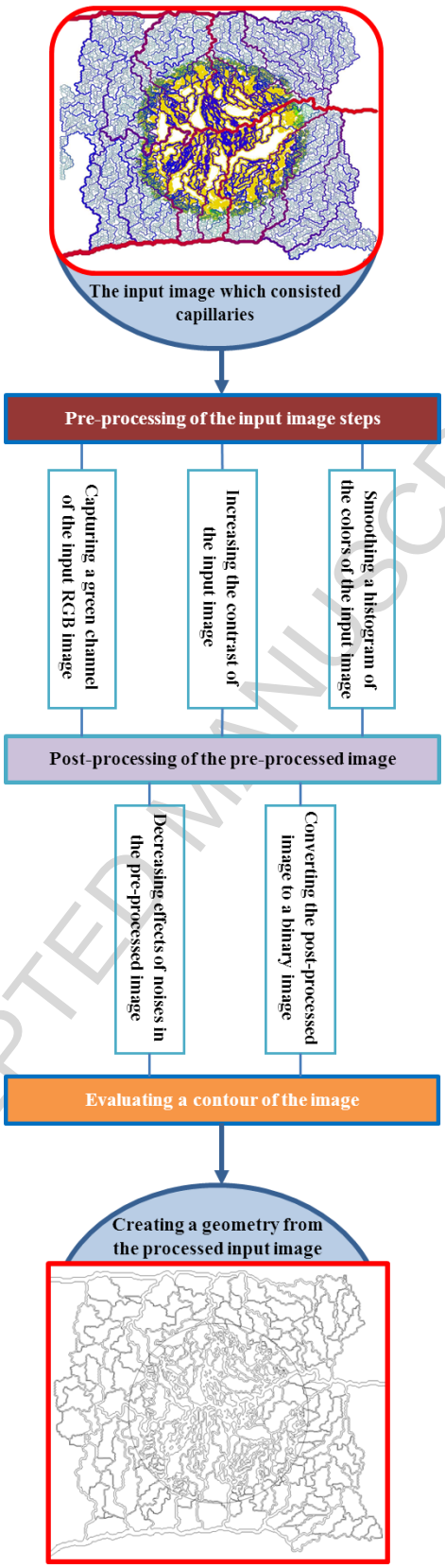

Fig. 3. Step by step description of image-processing procedure applied to the input image

2.3. Model geometry, computational domain, and boundary conditions

After image-processing, computational domain is considered as 2-dimensional rectangular normal tissue with the dimension of 1.8 cm × 1.6 cm and tumor has the diameter of 1 cm, as is shown in Fig. 4. Also, there exist three parent vessels which capillary network grows from them.

In the current study, a bolus injection of chemotherapy drug is modeled so that the concentration at the inlet of the vascular network decreases exponentially, as bellowing (Sefidgar et al., 2015):

$$C_p = \exp(-t/K_d) \quad (12)$$

K_d is a time constant that describes the exponential decay in the blood and corresponds to the blood half-life. In this study, it is assumed that the process of drug delivery is modeled instantly after the drug distribution within the capillaries reached to uniform state.

Due to having 2-dimensional geometry for capillary network, the pipe flow model (which is used for 1-dimensional geometries) cannot be used and therefore, blood flow is assumed to be modeled as a laminar flow (Asgari et al. 2018). For blood flow modeling, the pressure value of inlet and outlet parent vessels are as follows:

$P_{\text{Inlet},1}$ =25 mmHg $P_{\text{Inlet},2}$ =25 mmHg $P_{\text{Outlet},1}$ =10 mmHg

For the boundary between tumor and normal tissue, continuity of the IFV, IFP, and also concentration and its flux are considered as appropriate boundary conditions for inner boundary; where Ω^- and Ω^+ demonstrate the tumor and normal tissue at the boundary. Boundary conditions of the presented investigations are outlined in Table 3. For outer boundary, where the interstitial pressure is constant; the boundary condition of Dirichlet-type must be applied (Soltani and Chen, 2011), and for concentration, the open boundary condition is used (Sefidgar et al., 2014a).

Table 3. Boundary conditions employed for the present study

Region	Boundary condition	
	Fluid flow	**Concentration**
Center of the tumor	$\nabla P_i = 0$ *for r=0*	$D_{eff}\nabla C + v_i C = 0$ *for r=0*
Inner boundary	$-k_t \nabla P_i\big\|_{\Omega^-} = -k_n \nabla P_i\big\|_{\Omega^+}$	$(D^t_{eff}\nabla C + v_i C)C_i\big\|_{\Omega^-} = (D^n_{eff}\nabla C + v_i C)C_i\big\|_{\Omega^+}$
	$P_i\big\|_{\Omega^-} = P_i\big\|_{\Omega^+}$	$C_i\big\|_{\Omega^-} = C_i\big\|_{\Omega^+}$
Outer boundary	P_i = Constant	$-n \cdot \nabla C = 0$

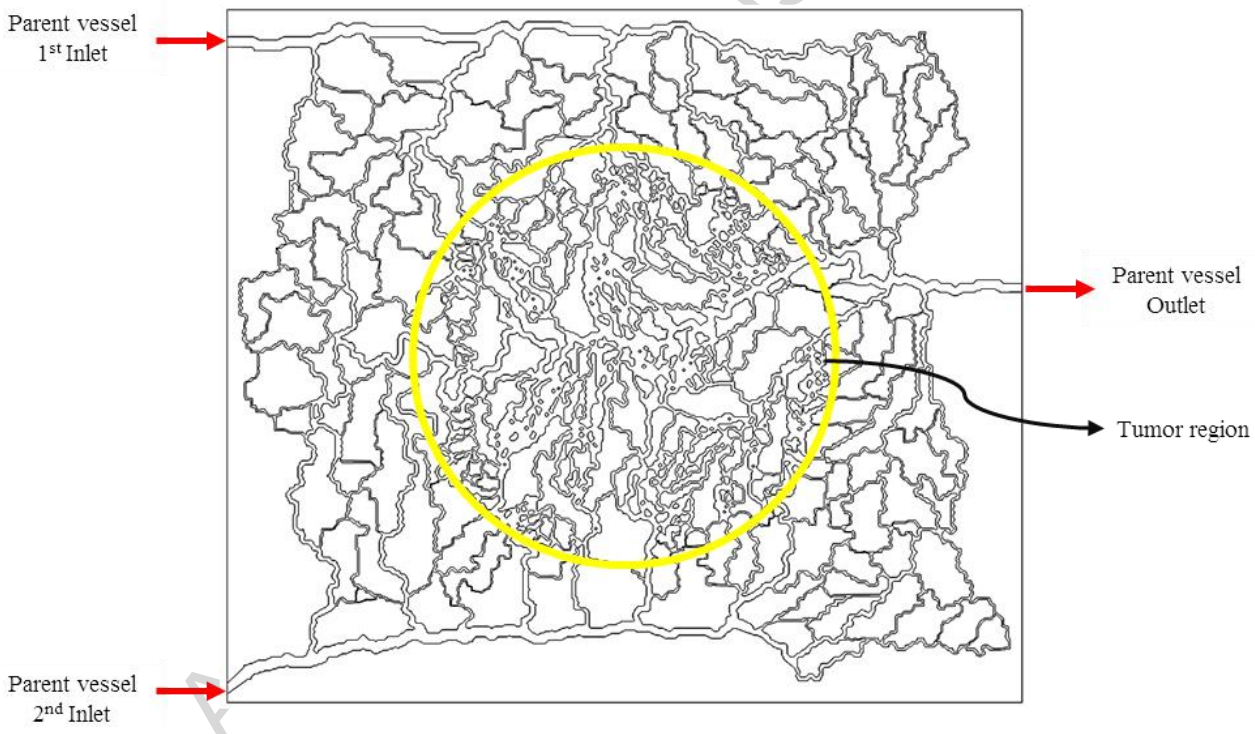

Fig. 4. Computational domain and boundary conditions of the current study which includes tumor, normal tissue, and microvascular network

2.4. Solution strategy

The general flowchart of solution strategy used to describe the simulation procedure of

drug delivery to solid tumor is shown in Fig. 5. First, computational domain is generated based on the input image. Then, there is two different phases of the solution: steady-state phase and time-dependent one. Laminar intravascular flow, IFV, and IFP are modeled in steady-state phase. In time-dependent phase, by using the information achieved from the previous steps, drug concentrations (C_F, C_B, and C_{INT}) and fraction of killed cells (S_F) are modeled.

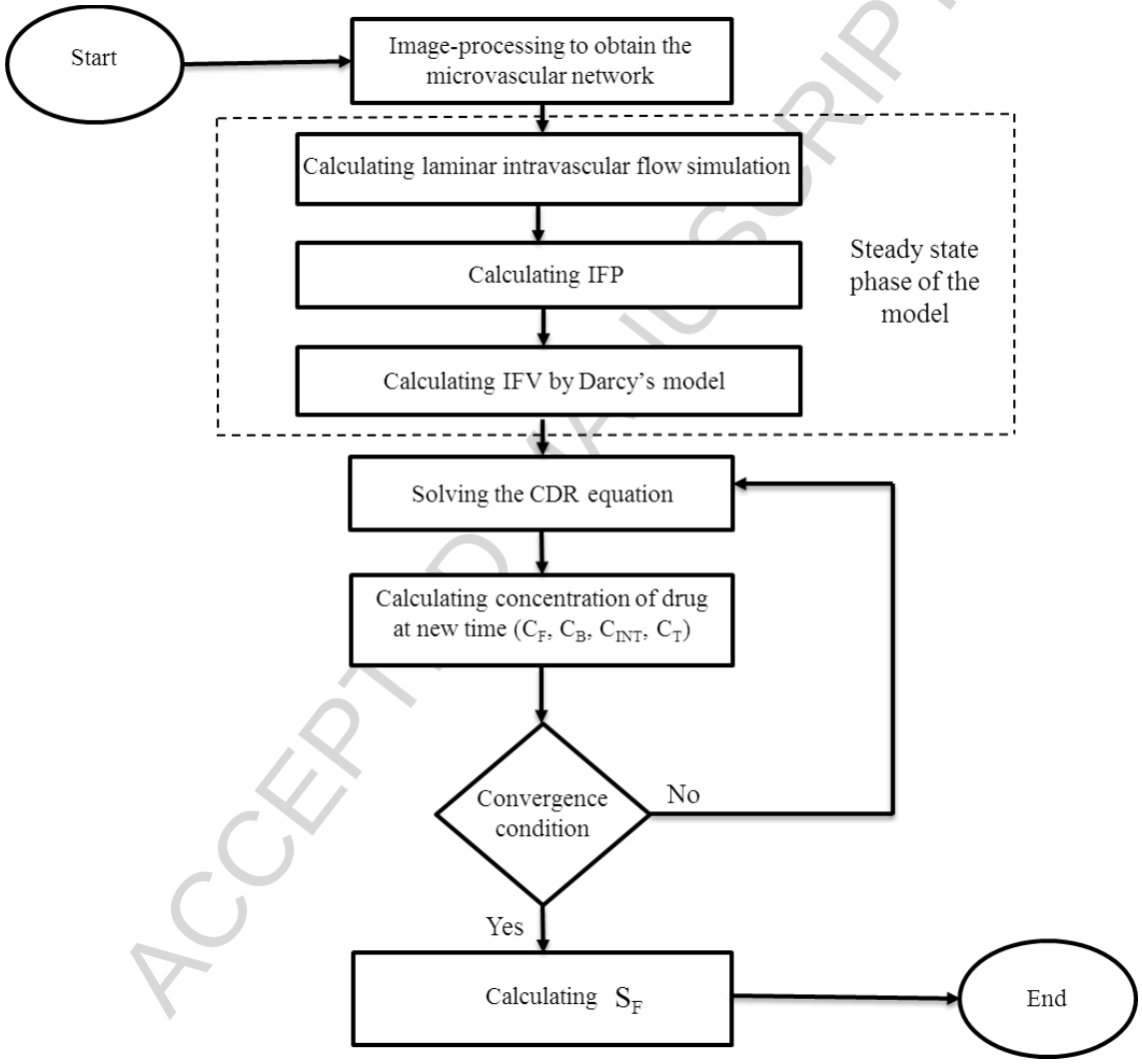

Fig. 5. The flowchart used to describe the simulation procedure of drug delivery to solid tumor

2.5. Grid independency test

Grid independency test is performed to show the impact of change in the number of mesh

elements on the simulation results. The appropriate number of elements is chosen by a trade-off between the cost of computational resources and the results of numerical solution (Soltani et al., 2019; Mehryan et al., 2018; Zargar et al., 2016). When the finer mesh does not change the numerical results significantly, the refined mesh is considered as suitable mesh (Soltani et al., 2019, 2018). Five different versions of the computational mesh (coarse, normal, fine, finer, and extra fine) are created to evaluate the mesh independency. With fine mesh elements (which is 4 times the initial number of mesh elements), less than 2% variation in simulated drug concentration and fluid flow parameters is found. By increasing the number of mesh elements to finer and extra fine (that is 8 and 16 times the initial number of mesh elements, respectively), almost no variation in the drug concentration and fluid flow parameters is observed. Therefore, the fine mesh elements due to the lowest computational costs are used for the whole simulation. It is worth mentioning that free triangular mesh is used in the current study for both normal and tumorous tissue as shown in Fig. 6.

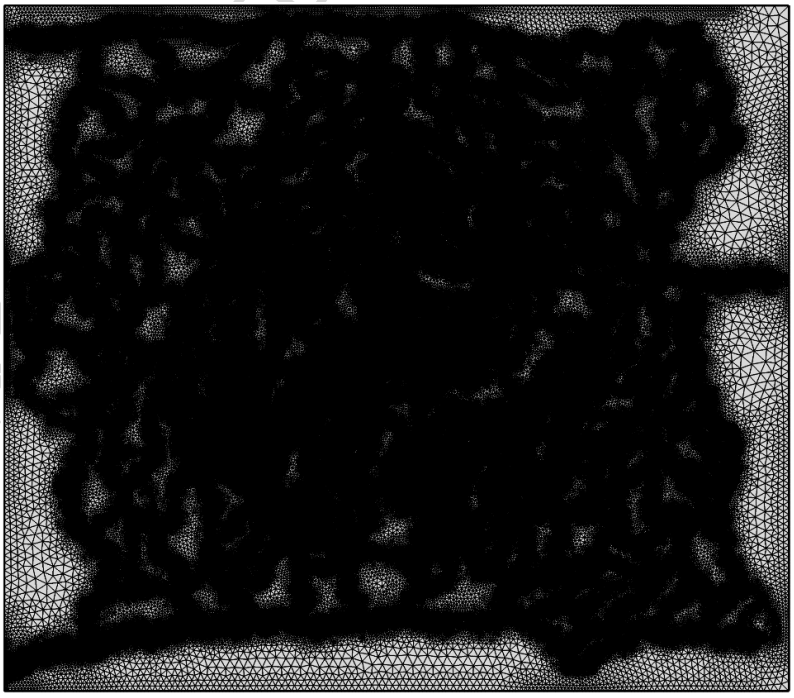

Fig. 6. Schematic view of optimum grid generation within a computational domain

3- Results and discussion

In the present study, an image-based solid tumor model employed for solving drug transport phenomenon based on CDR equations. Complex microvascular network adopted from three parent vessels are located within the tumor and normal tissue. In the following, the parameters of IFV, IFP, and concentration in tumor and normal tissue will be investigated in detail.

The intravascular blood pressure (IBP) and IFP distributions are illustrated in Figs. 7 (a) and (b), respectively. In the capillary network, the ratio of minimum IBP to maximum IBP is 0.4. This is in a good agreement to the predicted values of Sefidgar et al. (2015) and Cai et al. (2011) which is reported 0.4 and 0.3, respectively. The higher amount of IBP has both favorable and unfavorable influences on drug delivery. Because on one side, it increases the convective rate of drug transport from vessels and on the other side, increases the transvascular flow which terminates to increase in IFP in tumor region as one of the main obstacles of drug delivery to the tumor.

IFP in tumor and its surrounding tissue plays an important role in determining the convective drug transport between microvessels and interstitium driven by the gradient of transvascular pressure and also, drug convection in ECM. According to Fig. 7 (b), the IFP in tumor region has its highest value in comparison with normal tissue. The reason for elevated pressure in the tumor is the weakness of lymphatic system and the existence of high leakage of blood vessels. Also, in both tumor and normal tissues, in the areas where the vessels are closer together (higher microvascular density), the IFP is more. In other words, the predicted IFP is proportional to the microvascular density and reflects the heterogeneity in the tumor area. The heterogeneous microvascular network as source terms in interstitial fluid flow equation cause

non-uniform distribution of IFP in the tumor area. This effect is also reported by Stylianopoulos et al. (2013), and Wu et al. (2013). Here, the maximum value of IFP is 2.3 kPa, whereas the average value is approximately 1.8 kPa. These value is approximately close to the values reported by Boucher et al. (1990), Sefidgar et al. (2015), Soltani et al. (2017), and experimental results of Huber et al. (2005).

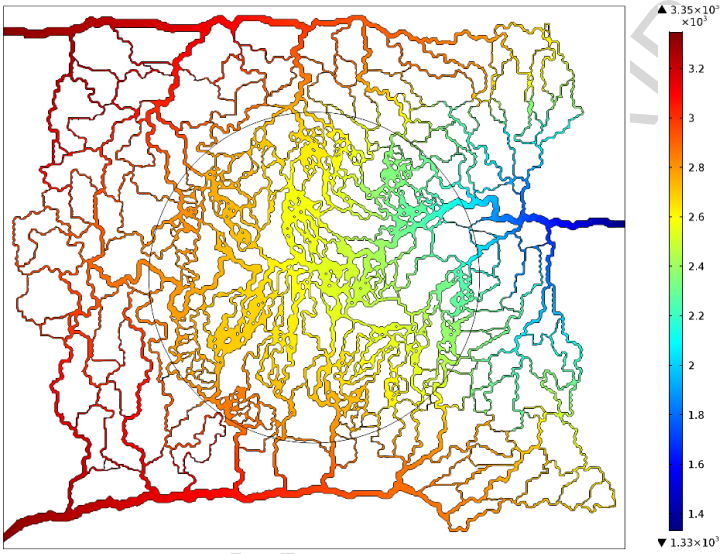

(a) Intravascular space

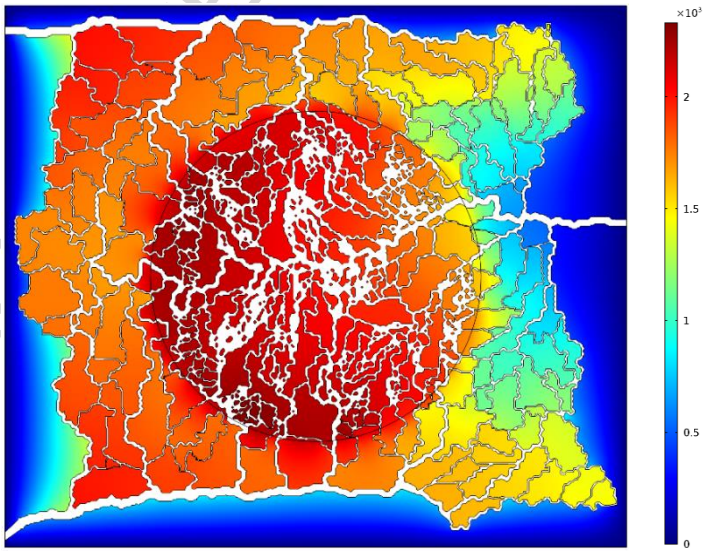

(b) Interstitial space

Fig. 7. Pressure distribution in (a) intravascular space (b) interstitial space

Velocity distributions in intravascular and interstitial spaces are shown in Figs. 8 (a) and (b). Blood velocity has the maximum value of 0.18 m/s in microvessels. As shown in the results, the IFV distribution is non-uniform. According to Darcy's law, in tissues, IFV depends on the gradient of IFP. Because IFP distribution is heterogeneous, the gradient of IFP and as a result, IFV have non-uniform distribution in tumor area as is reported in the works of Zhao et al. (2007) and Pishko et al. (2011). IFV has very low values in the whole computational domain. So, it can be said that the convection terms related to the interstitial flow are negligible (Soltani et al., 2017). In previous works (Zhao et al., 2007; Soltani et al., 2015), it is shown that these terms only affect on specific shapes and small sizes of tumors. The maximum value of IFV occurs at the tumor boundary, which is almost matched to the presented value of Sefidgar et al. (2015) and Pishko et al. (2011), and close to the measured values of Butler et al. (1975).

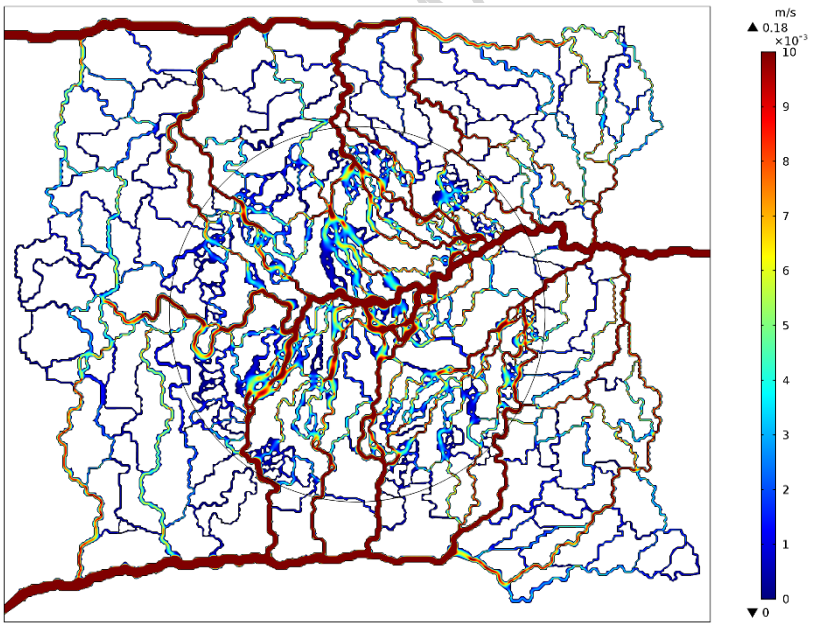

(a) Intravascular space

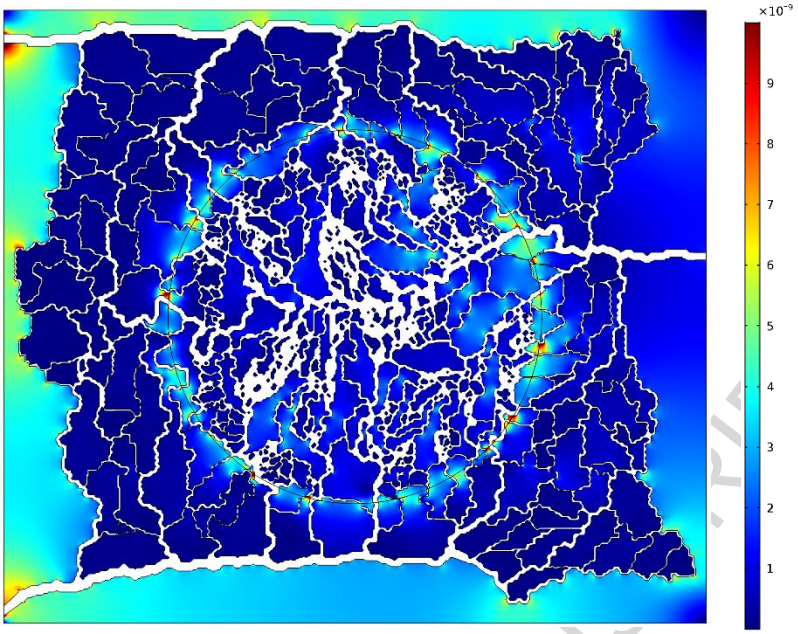

(b) Interstitial space

Fig. 8. Velocity distribution in (a) Intravascular space (b) Interstitial space

Figs. 9 (a)-(d) show the distribution of C_F, C_B, C_{INT}, and C_{TOT}, 1-hour after the drug has been injected, respectively. The results show that at this time, the value of bounded drug is more than the others, which indicates that due to convection and diffusion mechanisms, the free drug in ECM is converted to the bounded drug, gradually. In addition, during the same period, bounded drug also gradually develops into internalized drug.

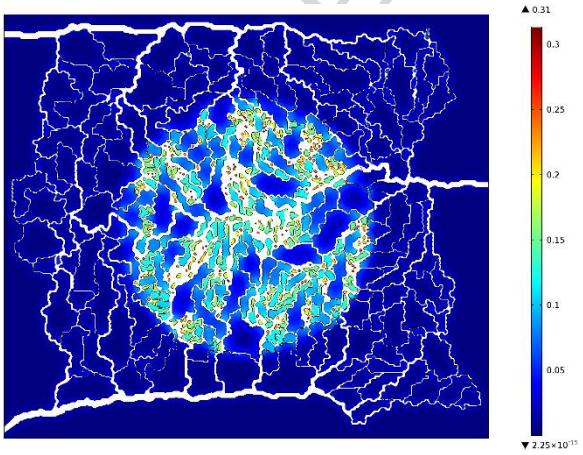

(a) C_F

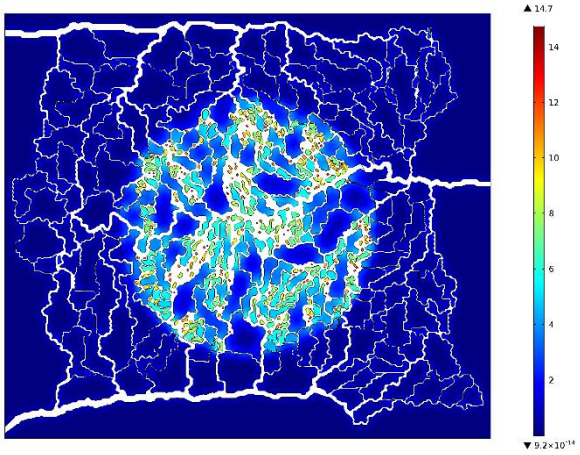

(b) C_B

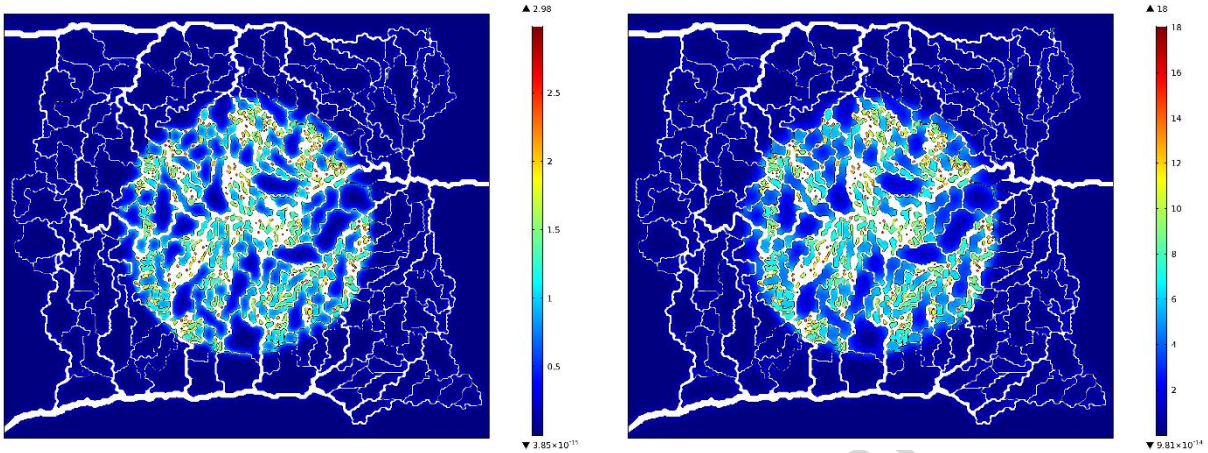

(c) C_{INT} (d) $C_{TOT}= C_F+C_B+C_{INT}$

Fig. 9. Distribution of different drug concentrations (C_F, C_B, C_{INT}, and C_{TOT}), 1-hour post-injection

In order to better demonstrate the spatio-temporal variation of drug concentration within the tumor, a non-dimensional illustration of different drug concentrations (i.e. C_F, C_B, C_{INT}, and C_{TOT}) are shown in Fig. 10. The values C_F , C_B , C_{INT} and C_{TOT} are the dimensionless forms of C_F, C_B, C_{INT}, and $C_{TOT,}$ respectively. Each parameter has been calculated by dividing the related concentration at a given point within the geometry by the maximum value of concentration within the entire domain, at a designated time. It is worth mentioning that total drug concentration is defined as a sum of three concentrations (free, bound, and internalized). In the beginning, the drug molecules are located in the blood microvessels but they are quickly transmitted to the tissue. After a relatively long time, the drug molecules are transmitted to the next regions of the domain through the mechanisms of convection and diffusion. C_F is dominant at early time steps. As the time goes ahead, C_B and C_{INT} are increasing gradually because of converting the free drug molecules to the bound and then, internalized molecules by means of binding and internalization processes. It is significant that free drug and bound drug concentration changes are going in the opposite directions. Also, it is obvious that drug concentration in the tumor area is more than the normal tissue in all snapshots of the tumor. The

maximum value of total concentration occurs in tumor region. This value is several times higher than the concentration in the normal tissue around it. The dependency of concentration to the vascular network structure is visible, so that, regions with a higher vascular density have a higher concentration compared to the other regions which there is no or there are just a few blood vessels.

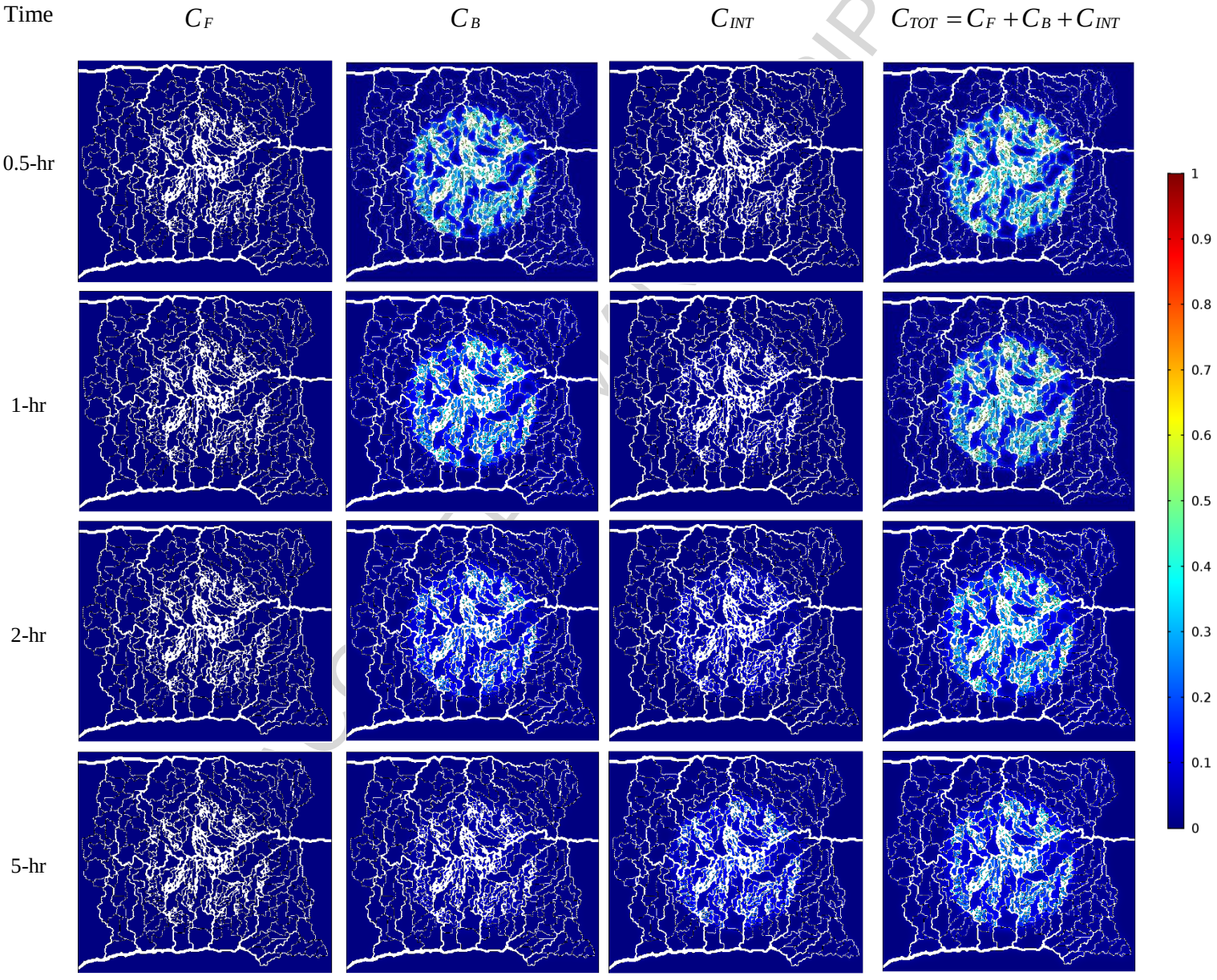

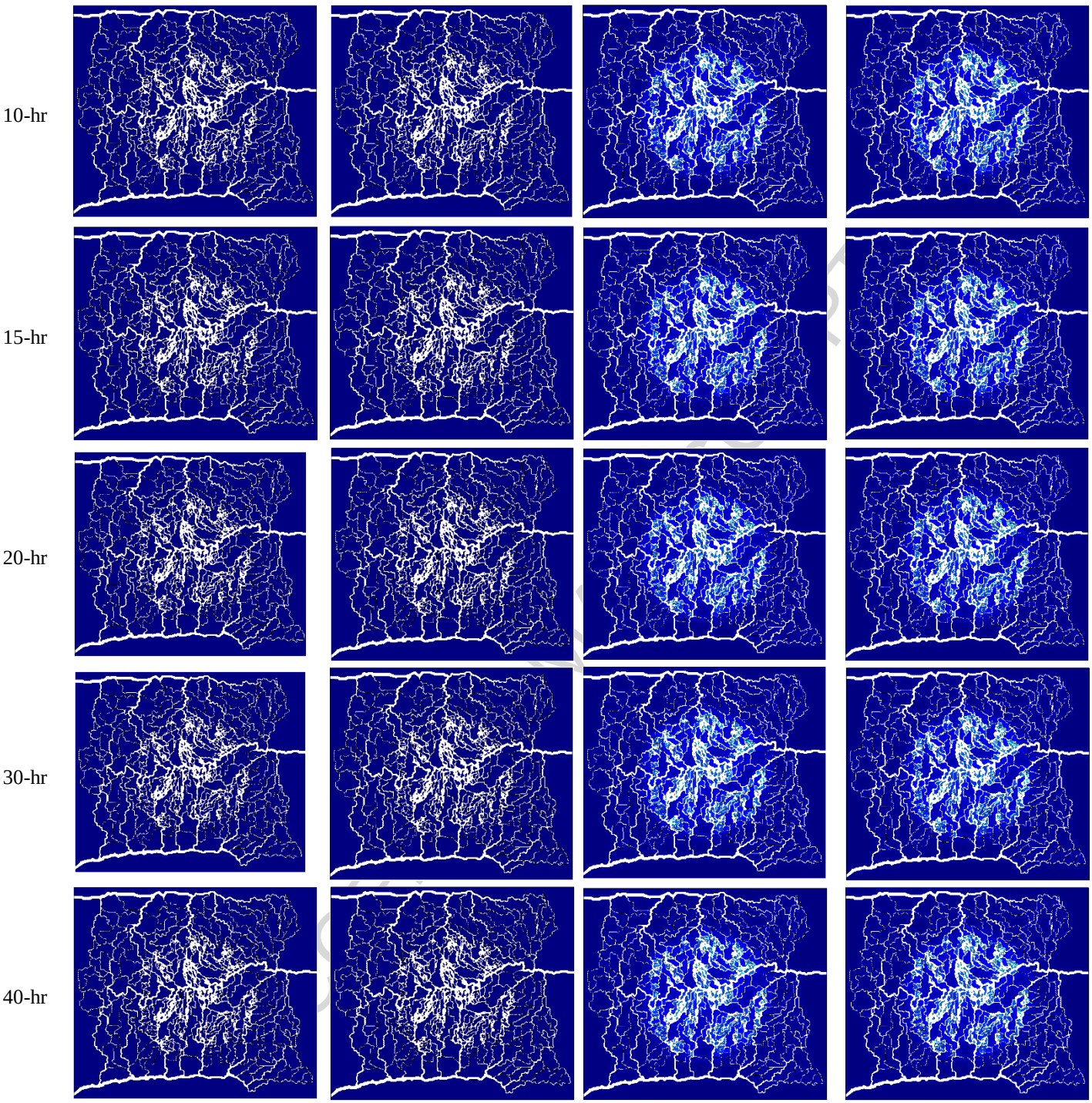

Fig. 10. Spatio-temporal distribution of non-dimensional concentration (C_F, C_B, C_{INT}, and C_{TOT}) at different times post-injection.

Fig. 11 represents different time-variant concentration profiles of the drug across the tumor and normal tissue. Average free, bound, internalized, and total drug concentration are

investigated in whole domain including tumor and normal tissue. In the beginning, total concentration increases with time according to the increase of plasma concentration and the source terms of drug extravasation. The maximum amount of average concentration occurs at a few minutes post-injection. After the end of the injection, the free and bound concentrations start falling immediately. At after approximately 30-hr post-injection, the average drug concentration is reached to a constant value. This trend generally exists for free and bound drug concentrations in both tumorous and normal tissues. The only difference is that the bound and free drug concentrations are reached to zero value. The internalized drug concentration increases over time and reaches a constant value after a specified time. By comparing the average concentration in tumor and normal tissue regions, it can be concluded that the highest amount of concentration occurred in the tumor region. The reason for this phenomenon is the higher permeability of the blood vessels in tumor compared to normal tissue.

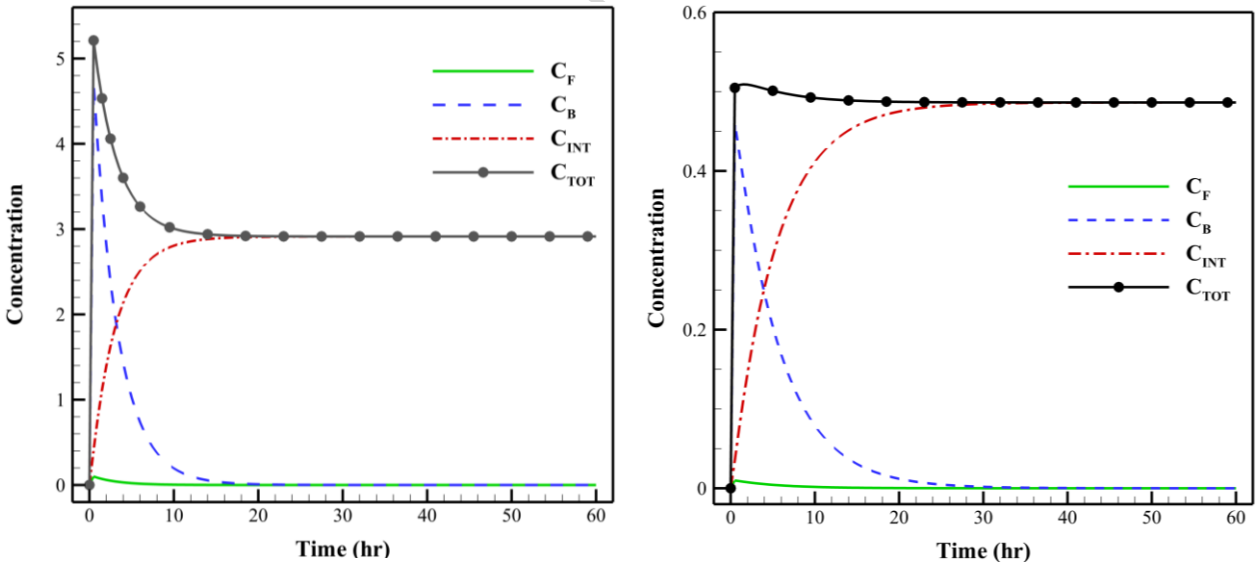

(a) Tumor (b) Normal tissue

Fig. 11. Different time-variant concentration profiles of the drug across the (a) Tumor (b) Normal tissue

To check the concentration changes in the computational domain, five different cut-lines are selected and shown in Fig. 12. The trend of concentration changes in all cut-lines is exactly

the same as in the general trend in Fig. 11, as demonstrated in Fig. 13. Similarly, for cut-lines 5 and 2, which pass through the center of the tumor, concentration has the maximum values. Cut-line 4 which located in normal tissue region has the minimum value compared to the other ones. Moreover, low density of microvessels can affect the average concentration value so that, the value of cut-line 1 is lower than the cut-line 3. Therefore, the cut-lines which located in tumor region and also near the well-vascularized regions have the higher amount of concentration.

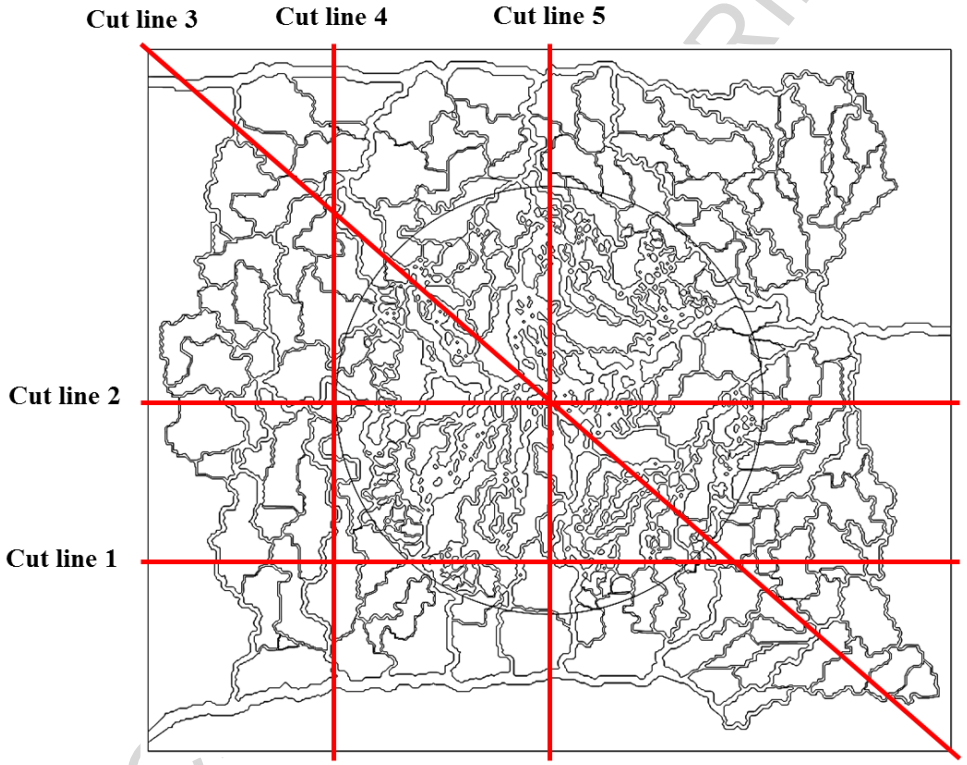

Fig. 12. The location of five different cut lines in computational domain

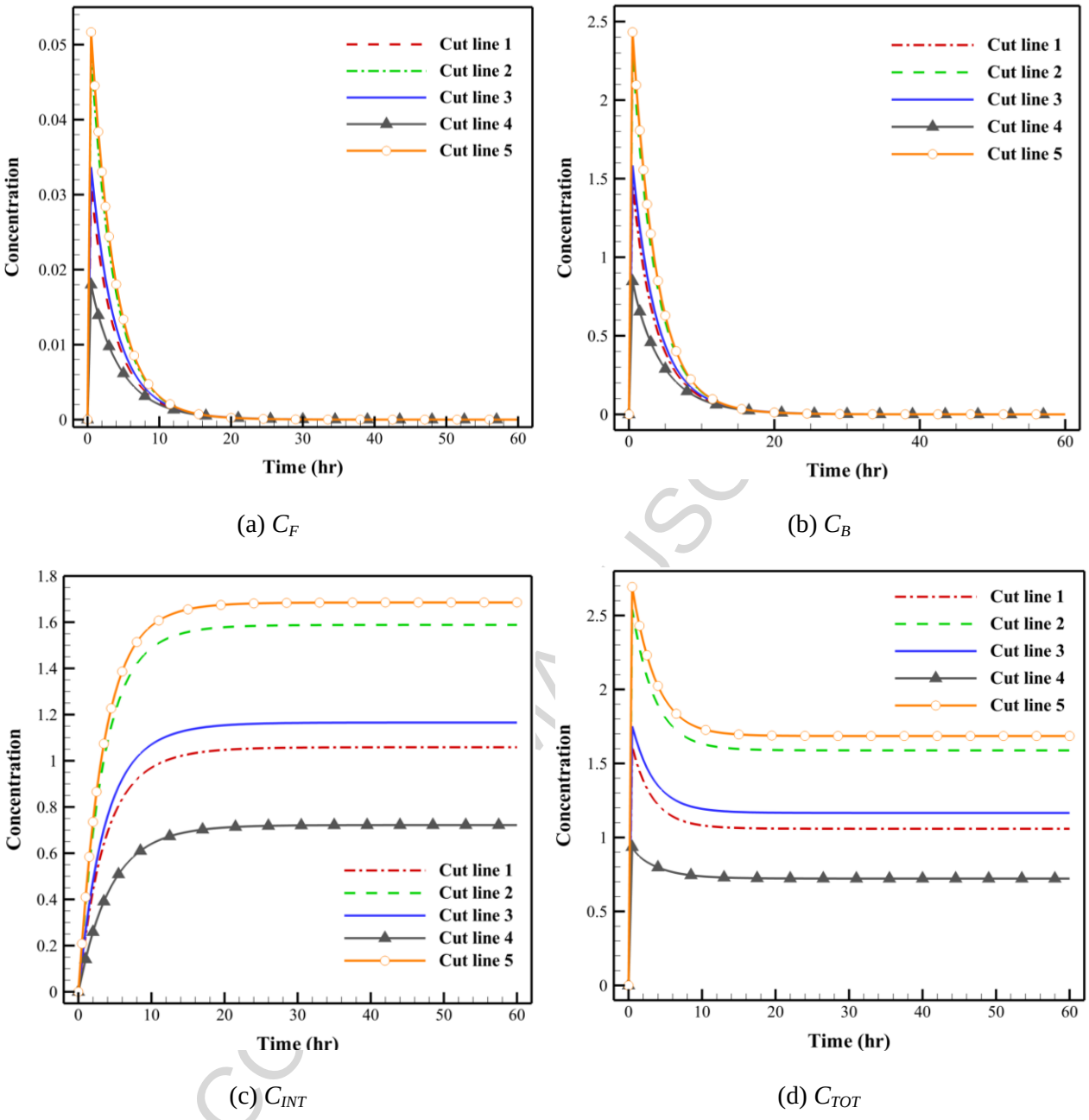

(a) C_F (b) C_B

(c) C_{INT} (d) C_{TOT}

Fig. 13. Variations of different concentrations in five determined cut-lines

The killing ability of the drug for tumor cells and also, side effects of the drug in damaging surrounding tissue play an important role in selecting an efficient chemotherapy drug. Fig. 14. shows the fraction of killed cells in the tumor and normal tissue over time during the treatment. The overall rate of killed cells is about 78.65% after treatment with doxorubicin. In addition to the effectiveness of killing cancer cells, the side effects to normal tissues during

chemotherapy should also be considered. The side effects of drug injection act as a limiting factor for drug delivery, because if side effects in a healthy tissue or other tissues exceed a specific amount, they will cause serious damage and even gradual death of the tissues and ultimately organs. Therefore, the fraction of killed cells for normal tissue is also investigated. From Fig. 14, the rate of killed cells for a normal tissue after treatment of doxorubicin is about 24.94%. It is worth mentioning that the anticancer drug kills both cancer and normal cells without any distinction. On the other hand, delivery outcomes of doxorubicin obtained by modeling are compared with simulations carried out by Stylianopoulos et al. (2015). Results obtained from current modeling for the fraction of killed cells, were in good agreements with those reported by (Stylianopoulos et al., 2015). Error between the simulation results and literature are mainly due to difference in the geometry of heterogeneous capillary network and computational domain, and considering the lymphatic system in tumor region.

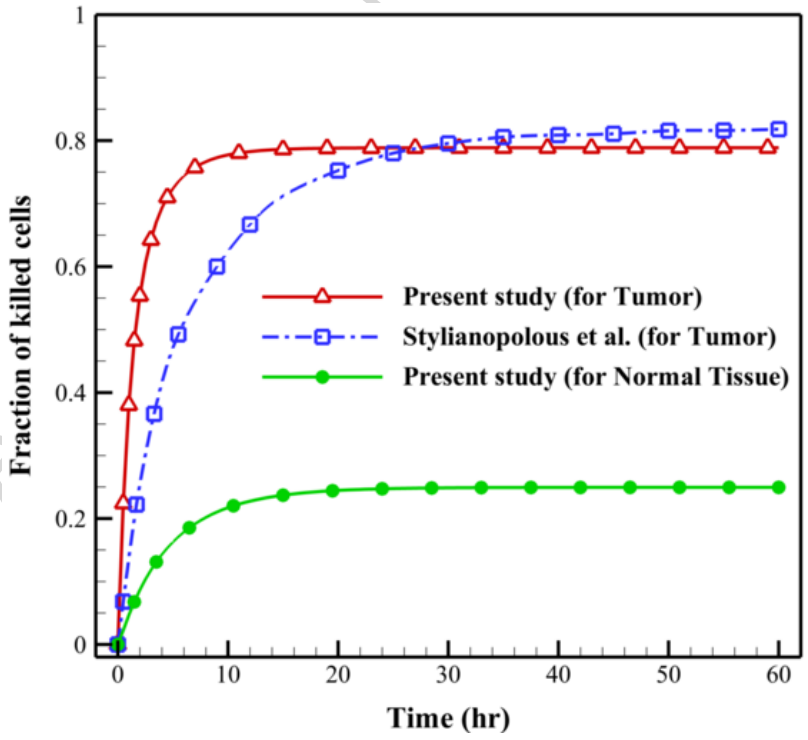

Fig. 14. The fraction of killed cells in the tumor and normal tissue over time

By incorporating heterogeneous microvessel's density in a tumor model, the current study has provided more percipience into the influence of non-uniform distribution of the tumor microvasculature on drug delivery. The effects of intravascular transport and geometric characteristics of tumor microvasculature are also considered. This model takes into account the chemotherapy release, its binding, and uptake by cancer cells. In general, results indicate the dependency of the drug distribution on both time and space. Also, results show that the concentration changes with the microvasculature density. Moreover, the fraction of killed cells is presented as a criterion for evaluating the drug efficacy.

The tumor microenvironment is very complicated to be precisely represented by using a single mathematical model. So, the mathematical modeling employed in this study involves some assumptions. The main assumption is considering 2-dimensional tumor model instead of a full 3-dimensional model. According to the works of Zhan et al. (2014) on the prostate tumor, the effect of 3-dimensional on spatial-mean parameters like internalized drug is ignorable. This is in agreement with the study of Teo et al. (2005) who found qualitatively the same results between 2-dimensional and 3-dimensional models of a brain tumor. A 2-dimensional region is also employed in other works such as Jain and co-authors (Stylianopoulos et al., 2013, 2015; Mperkis et al., 2017; Stylianopoulos and Jain, 2013), Stephanou and co-authors (2005), Soltani and co-authors (2015, 2017, 2018), and Chou et al. (2017). Another assumption is such that the uniform transport properties and also, uniform tumor cell density are assumed without considering the heterogeneity of intra-or inter-tumor. Moreover, due to using an image as input for capillary networks, the authors had to assume the laminar flow in capillaries. In general, because of the limitations and the lack of experimental validation, the model predictions described in the present study should be regarded as qualitative rather than quantitative.

Conclusion

The present approach bridges the techniques of image analysis for reconstructing the capillary network and CDR modeling for extracting the various measures of fluid properties including IFP, IFV, and drug concentration. The coupling mathematical model which solves both blood flow in the capillary network, as well as the fluid flow in the interstitial space, is employed to calculate the distribution of IFP and IFV. Then, a comprehensive model based on CDR equations is used to simulate the drug binding and uptake by tumor cells. Efficacy of anticancer drug and also, side effects of the drug on normal tissue are evaluated based on the fraction of killed cells parameter by using the predicted intracellular drug concentration. The presented computational model provides the necessary first steps toward personalized medicine. By considering such image-based model, numerical simulations will shed more light on important mechanisms of drug delivery inside the tumor and, simultaneously, suggest a better and more practical evaluation of the tumor treatment. The main limitations of current model are: using 2-dimensional tumor model instead of a full 3-dimensional model, considering static network for capillaries, assuming the laminar flow model for blood flow through microvascular network, and considering uniform transport properties for normal and tumor tissues.

References

Abdallah, M.B., Malek, J., Azar, A.T., Montesinos, P., Belmabrouk, H., Monreal, J.E., Krissian, K., 2015. Automatic extraction of blood vessels in the retinal vascular tree using multiscale medialness. J. Biomedical Imaging. 2015, Article ID 519024.

Anderson, A.R.A., Chaplain, M.A.J., 1998. Continuous and discrete mathematical models of tumor-induced angiogenesis. Bulletin of mathematical biology. 60, 857– 899.

Anderson, A., Chaplain, M., McDougall, S., 2012. A hybrid discrete-continuum model of tumor

induced angiogenesis. In: Jackson TL, Editor. Modeling Tumor Vasculature. New York, NY: Springer, pp. 105–134.

Asgari, H., Soltani, M., Sefidgar, M., 2018. Modeling of FMISO [F18] nanoparticle PET tracer in normal-cancerous tissue based on real clinical image. Microvasc. Res. 118, 20–30.

Baxter, L.T., Jain, R.K., 1989. Transport of fluid and macromolecules in tumors. (I) Role of interstitial pressure and convection. Microvasc. Res. 37, 77–104.

Baxter, L.T., Jain, R.K., 1990. Transport of fluid and macromolecules in tumors. (II) Role of heterogeneous perfusion and lymphatics. Microvasc. Res. 40, 246–263.

Baxter, L.T., Jain, R.K., 1991. Transport of fluid and macromolecules in tumors (III) Role of binding and metabolism. Microvasc. Res. 41, 5–23.

Bhandari, A., Bansal, A., Singh, A., Sinha, N., 2018. Numerical study of transport of anticancer drugs in heterogeneous vasculature of human brain tumors using dynamic contrast enhanced-magnetic resonance imaging. J. Biomech. Eng. 140, 051010.

Boucher, Y., Baxter, L.T., Jain, R.K., 1990. Interstitial pressure gradients in tissue-isolated and subcutaneous tumors: implications for therapy. Cancer Res. 50, 4478–4484.

Butler, T.P., Grantham, F.H., Gullino, p.m., 1975. Bulk transfer of fluid in the interstitial compartment of mammary tumors, Cancer Res. 35, 3084-3088.

Cai, Y., Xu, S., Wu, J., Long, Q., 2011. Coupled modelling of tumour angiogenesis, tumour growth and blood perfusion. J. Theor. Biol. 279, 90–101.

Chaudhuri, S., Chatterjee, S., Katz, N., Nelson, M., Goldbaum, M., 1989. Detection of blood vessels in retinal images using two-dimensional matched filters. IEEE Trasactions on Medical Imaging. 8, 263–269.

Chou, C.Y., Chang, W.I., Horng, T.L., Lin, W.L., 2017. Numerical modeling of nanodrug

distribution in tumors with heterogeneous vasculature. PLoS ONE. 12, e0189802.

Curry, F.E., 1984. Mechanics and thermodynamics of transcapillary exchange. In: Renkin EM, Michel CC, editors. Handb. Physiol, section 2. American Physiological Society.

Dewhirst, M.W., Secomb, T.W., 2017. Transport of drugs from blood vessels to tumour tissue. Nature Reviews Cancer. 17, 738–750.

Eikenberry. S., 2009. A tumor cord model for Doxorubicin delivery and dose optimization in solid tumors. Theor. Biol. Med. Model. 6, 16-4862-6-16.

El-Kareh. A.W., Secomb, T.W., 2005. Two-mechanism peak concentration model for cellular pharmacodynamics of Doxorubicin. Neoplasia. 7, 705-713.

Huber, P.E., Bischof, M., Heiland, S., Peschke, P., Saffrich, R., Gro, H., Lipson, K.E., Abdollahi, A., 2005. Trimodal cancer treatment: beneficial effects of combined antiangiogenesis, radiation, and chemotherapy. Cancer Res. 65, 3643–3655.

Jain, R.K., Baxter, L.T., 1988. Mechanisms of heterogeneous distribution of monoclonal antibodies and other macromolecules in tumors: significance of elevated interstitial pressure. Cancer Res. 48, 7022–7032.

Jain, R.K., 1997. Delivery of molecular and cellular medicine to solid tumors. Microcirculation. 4, 1–23.

Janko, T.P., Beichel, R., Bischof, H., 2005. Multi-scale medialness for robust segmentation of 3D tubular structures. The 10th Computer Vision with Workshop, The Austrian Science Fund (FWF) under the grants P17066-N04.

Kerr, D.J., Kerr, A.M., Freshney, R.I., Kaye, S.B., 1986. Delivery of molecular and cellular medicine to solid tumors. Biochem Pharmacol. 35, 12817–2823.

Malek, J., Azar, A.T., Tourki, R., 2015, Impact of retinal vascular tortuosity on retinal

circulation. Neural Comput. Appl. 26, 25–40.

Meghdadi, N., Soltani, M., Niroomand-Oscuii, H., Ghalichi, F., 2016. Image based modeling of tumor growth. Australas. Phys. Eng. Sci. Med. 39, 601-613.

Mehryan, S.A.M., Kashkooli, F.M., Soltani, M., 2018. Comprehensive study of the impacts of surrounding structures on the aero-dynamic performance and flow characteristics of an outdoor unit of split-type air conditioner. Buil. Sim. 11, 325–337.

Mpekris, F., Baish, J.W., Stylianopoulos, T., Jain, R.K., 2017. Role of vascular normalization in benefit from metronomic chemotherapy. PNAS. 114, 1994–1999.

Pishko, G.L., Astary, G.W., Mareci, T.H., Sarntinoranont, M., 2011. Sensitivity analysis of an image-based solid tumor computational model with heterogeneous vasculature and porosity. Ann. Biomed. Eng. 39, 2360-2373.

Rangayyan, R.M., Oloumi, F., Eshghzadeh-Zanjani, P., Ayres, F.J., 2007. Detection of blood vessels in the retina using Gabor filters. The 20th Canadian Conference on Electrical and Computer Engineering (CCECE ’07), pp. 717– 720, Vancouver, Canada.

Sefidgar, M., Soltani, M., Raahemifar, K., Bazmara, H., Nayinian, S., Bazargan, M., 2014a. Effect of tumor shape, size, and tissue transport properties on drug delivery to solid tumors. J. Biol. Eng. 8, 12.

Sefidgar, M., Soltani, M., Bazmara, H., Mousavi, M., Bazargan, M., Elkamel, A., 2014b. Interstitial flow in cancerous tissue: effect of considering remodeled capillary network. J. Tissue Sci. Eng. 4, 1–8.

Sefidgar, M., Soltani, M., Raahemifar, K., Sadeghi, M., Bazmara, H., Bazargan, M., Mousavi, S.M., 2015. Numerical modeling of drug delivery in a dynamic solid tumor microvasculature. Microvasc. Res. 99, 43–56.

Soltani, M., Chen, P., 2011. Numerical modeling of fluid flow in solid tumors. PLoS ONE 6, 1-15.

Soltani, M., 2012. Numerical modeling of drug delivery to solid tumor microvasculature. PhD thesis, Chem. Eng. (Nanotechnology), Waterloo, Ontario, Canada.

Soltani, M., Chen, P., 2012. Effect of tumor shape and size on drug delivery to solid tumors. J. Biol. Eng. 6, 4.

Soltani, M., Chen, P., 2013. Numerical modeling of interstitial fluid flow coupled with blood flow through a remodeled solid tumor microvascular network. PLoS ONE 8, e67025.

Soltani, M., Rahpeima, R., M. Kashkooli, F., 2019. Breast cancer diagnosis with a microwave thermoacoustic imaging technique—a numerical approach. Med. Biol. Eng. Comput., In Press.

Soltani, M., Sefidgar, M., Casey, M.E., Wahl, R.L., Subramaniam, R.M., Rahmim, A. 2014. Comprehensive modeling of the spatiotemporal distribution of PET tracer uptake in solid tumors based on the convection-diffusion-reaction equation. In: 21th IEEE Nuclear Science Symposium Medical Imaging Conference Washington State Convention Center, Seattle, WA USA.

Soltani, M., Sefidgar, M., Bazmara, H., Subramaniam, R., Rahmim, A., 2015. Effect of tumor shape and size on drug delivery. J. Nucl. Med. 56, 1220.

Soltani, M., Bazmara, H., Sefidgar, M., Subramaniam, R., Rahmim, A., 2015. study on the impact of tumor shape and size on drug delivery to pancreatic tumors. Med. Phys. 42, 3220.

Soltani, M., Sefidgar, M., Bazmara, H., Casey, M.E., Subramaniam R.M., Wahl, R.L., Rahmim, A., 2017. Spatiotemporal distribution modeling of PET tracer uptake in solid tumors. Ann. Nucl. Med. 31, 109–124.

Soltani, M., Dehghani-Sanij, A., Sayadnia, A., Kashkooli, F.M., Gharali, K., Mahbaz, S.B., Dusseault, M.B., 2018. Investigation of airflow patterns in a new design of wind tower with a

wetted surface. Energies. 11, 1–23.

Shamsi, M., Sedaghatkish, A., Dejam, M., Saghafian, M., Mohammadi, M., Sanati-Nezhad, A., 2018. Magnetically assisted intraperitoneal drug delivery for cancer chemotherapy. Drug Delivery. 25, 846–861.

Stephanou, A., McDougall, S., Anderson, A., Chaplain, M., 2005. Mathematical modeling of flow in 2D and 3D vascular networks: Applications to antiangiogenic and chemotherapeutic drug strategies. Math. Comput. Model. 41, 1137–1156.

Steuperaert, M., D'Urso Labate G.F., Debbaut Ch., De Wever, O., Vanhove, Ch., Ceelen, W., Segers, P., 2017. Mathematical modeling of intraperitoneal drug delivery: simulation of drug distribution in a single tumor nodule. Drug Delivery. 24, 491–501.

Sofka M., Stewar, C.V., 2005. Retinal vessel extraction using multiscale matched filters confidence and edge measures. Tech. Rep., Department of Computer Science, Rensselaer Polytechnic Institute, New York, USA.

Strisciuglio, N., Azzopardi, G., Vento, M., Petkov N., 2015. Multiscale blood vessel delineation using B-COSFIRE filters, International Conference on Computer Analysis of Images and Patterns. Springer, pp. 300-312.

Stylianopoulos, T., Jain, R.K., 2013. Combining two strategies to improve perfusion and drug delivery in solid tumors. PANS. 110, 18632–18637.

Stylianopoulos, T., Soteriou, K., Fukumura, D., Jain, R.K., 2013. Cationic nanoparticles have superior transvascular flux into solid tumors: insights from a mathematical model. Ann. Biomed. Eng. 41, 68–77.

Stylianopoulos, T., Economides, E.A., Baish, J.W., Fukumura, D., Jain, R.K., 2015. Towards optimal design of cancer nanomedicines: multi-stage nanoparticles for the treatment of solid

tumors. Ann. Biomed. Eng. 43, 2291–2300.

Stylianopoulos, T., Munn, L.L., Jain, R.K., 2018. Reengineering the Physical Microenvironment of Tumors to Improve Drug Delivery and Efficacy: From Mathematical Modeling to Bench to Bedside. Trends in Cancer 4, 292–319.

Tan, W.H.K., Wang, F., Lee, T., Wang, Ch.H., 2003.Computer simulation of the delivery of etanidazole to brain tumor from PLGA wafers: Comparison between linear and double burst release systems. Biotech. Bioeng. 82, 278–288.

Teo, Ch.S., Tan, W.H.K., Lee, T., Wang, Ch.H., 2005. Transient interstitial fluid flow in brain tumors: effect on drug delivery. Chem. Eng. Sci. 60, 4803-4821.

Welter, M., Bartha, K., Rieger, H., 2008. Emergent vascular network inhomogeneities and resulting blood flow patterns in a growing tumor. J. Theor. Biol. 250, 257–280.

Welter, M., Bartha, K., Rieger, H., 2009. Vascular remodelling of an arterio-venous blood vessel network during solid tumour growth. J. Theor. Biol, 259, 405–422.

Welter, M., Rieger, H., 2010. Physical determinants of vascular network remodeling during tumor growth. Eur. Phys. J. E. Soft Matter. 33, 149–163.

Welter, M., Rieger, H., 2013. Interstitial fluid flow and drug delivery in vascularized tumors: a computational model. PLoS One. 8e70395.

Wu, J., Long, Q., Xu, S., Padhani, A.R., Jiang, Y., 2008. Simulation of 3D solid tumour angiogenesis including arteriole, capillary and venule. J. Angiogenesis. 5, 1–23.

Wu, M., Frieboes, H.B., McDougall, S.R., Chaplain, M. a J., Cristini, V., Lowengrub, J., 2013. The effect of interstitial pressure on tumor growth: coupling with the blood and lymphatic vascular systems. J. Theor. Biol. 320, 131–151..

Wu, M., Frieboes, H.B., Chaplain M.A.J., McDougall, S.R., Cristini V., Lowengrub J.S., 2014.

The effect of interstitial pressure on therapeutic agent transport: Coupling with the tumor blood and lymphatic vascular systems. J. Theor. Biol. 355, 194–207.

Zargar, B., Kashkooli, F.M., Soltani, M., Wright, K.E., Ijaz, M.Kh., Sattar, S.A., 2016. Mathematical modeling and simulation of bacterial distribution in an aerobiology chamber using computational fluid dynamics. Am. J. Infect. Control. 44, S127– S137.

Zhan, W., Xu, X.Y., 2013. A mathematical model for thermosensitive liposomal delivery of Doxorubicine to solid tumour. Journal of Drug Delivery. 2013, Article ID: 172529..

Zhan, W., Gedroyc, W., Xu, X.Y., 2014. Effect of heterogeneous microvasculature distribution on drug delivery to solid tumour. J. Phys. D: Appl. Phys. 47, 475401.

Zhan, W., Gedroyc, W., Xu, X.Y., 2017. Spatiotemporal distribution modeling of PET tracer uptake in solid tumors. PLoS ONE. 12, e0172276.

Zhang, B., Zhang, L., Karray, F., 2010. Retinal vessel extraction by matched filter with first-order derivative of Gaussian. Comput. Biol. Med. 40, 438–445.

Zhang, B., Drapaca, C., Zhang, Zh., Zhang, Sh., Sun, Sh., Liu, H., 2017. Leakage Evaluation by Virtual Entropy Generation (VEG) Method. Entropy 20, 14.

Zhang, Zh., Jie, Xu, Hong, B., Chen, X., 2014. The effects of 3D channel geometry on CTC passing pressure – towards deformability-based cancer cell separation. Lab on a Chip 14, 2576.

Zhang, Zh., Chen, X., Xu, J., 2015. Entry effects of droplet in a micro confinement: Implications for deformation-based circulating tumor cell microfiltration. Biomicrofluidics 9, 024108.

Zhang, Zh., 2018. Modeling of fluid flow in capillary channels, Ph.D. Thesis, Pennsylvania State University, Pennsylvania, USA.

Zhao, J., Salmon, H., Sarntinoranont, M., 2007. Effect of heterogeneous vasculature on interstitial transport within a solid tumor. Microvasc. Res. 73, 224–236.

Highlights

- An imaged-based computational modeling of drug distribution is considered
- A comprehensive spatio-temporal drug delivery model in tumor and normal tissue is developed
- For more accuracy of the modeling, blood flow and interstitial flow are considered
- The fraction of killed cells is evaluated both for tumor and normal tissue